Published online 8 February 2013 *Nucleic Acids Research, 2013, Vol. 41, No. 6* ***3901–3914***
doi:10.1093/nar/gkt010

Crystal structure of Cex1p reveals the mechanism of tRNA trafficking between nucleus and cytoplasm

Kayo Nozawa[1], Ryuichiro Ishitani[1], Tohru Yoshihisa[2], Mamoru Sato[3], Fumio Arisaka[4], Shuji Kanamaru[4], Naoshi Dohmae[5], Dev Mangroo[6], Bruno Senger[7], Hubert D. Becker[7] and Osamu Nureki[1,*]

[1]Department of Biophysics and Biochemistry, Graduate School of Science, University of Tokyo, 2-11-16 Yayoi, Bunkyo-ku, 113-0032 Tokyo, Japan, [2]Department of Chemistry, Graduate School of Science, Nagoya University, Chikusa-ku, Nagoya 464-8602, Japan, [3]Graduate School of Nanobioscience, Yokohama City University, 1-7-29 Suehiro-cho, Tsurumi-ku, Yokohama, Kanagawa 230-0045, Japan, [4]Department of Life Science, Graduate School of Bioscience and Biotechnology, Tokyo Institute of Technology, Yokohama, Kanagawa, Japan [5]Biomolecular Characterization Team, RIKEN, 2-1 Hirosawa, Wako-shi, Saitama 351-0198, Japan, [6]Department of Chemistry and Biochemistry, Guelph-Waterloo Center for Graduate Work in Chemistry and Biochemistry, University of Guelph, Guelph, ON N1G 2W1, Canada and [7]Institut de Physiologie et Chimie Biologique, UMR 7156, 21 rue René Descartes, 67084 Strasbourg cedex, France

Received September 20, 2012; Revised December 11, 2012; Accepted December 20, 2012

ABSTRACT

In all eukaryotes, transcribed precursor tRNAs are maturated by processing and modification processes in nucleus and are transported to the cytoplasm. The cytoplasmic export protein (Cex1p) captures mature tRNAs from the nuclear export receptor (Los1p) on the cytoplasmic side of the nuclear pore complex, and it delivers them to eukaryotic elongation factor 1α. This conserved Cex1p function is essential for the quality control of mature tRNAs to ensure accurate translation. However, the structural basis of how Cex1p recognizes tRNAs and shuttles them to the translational apparatus remains unclear. Here, we solved the 2.2 Å resolution crystal structure of *Saccharomyces cerevisiae* Cex1p with C-terminal 197 disordered residues truncated. Cex1p adopts an elongated architecture, consisting of N-terminal kinase-like and a C-terminal α-helical HEAT repeat domains. Structure-based biochemical analyses suggested that Cex1p binds tRNAs on its inner side, using the positively charged HEAT repeat surface and the C-terminal disordered region. The N-terminal kinase-like domain acts as a scaffold to interact with the Ran-exportin (Los1p·Gsp1p) machinery. These results provide the structural basis of Los1p·Gsp1p·Cex1p·tRNA complex formation, thus clarifying the dynamic mechanism of tRNA shuttling from exportin to the translational apparatus.

INTRODUCTION

In all eukaryotes, transcription in the nucleus and translation in the cytoplasm are separated by the nuclear envelope (NE). Nuclear pore complexes (NPC) perforate the NE and allow the passage of macromolecules, such as proteins and RNAs. In the transport of these molecules, the nuclear export of tRNA is particularly important for bridging nuclear transcription and cytoplasmic translation. Eukaryotic tRNA genes are transcribed as precursor tRNAs (pre-tRNAs) by RNA polymerase III in the nucleus. These pre-tRNAs undergo further trimming at the 5′ and 3′ termini, intron splicing, base modification and the addition of the 3′-CCA terminus in the nucleus, and finally, the mature tRNAs are transported to the cytoplasmic translational machinery (1–3).

However, various studies have shown that the intron removal from yeast pre-tRNAs is catalyzed by tRNA splicing endonucleases located on the cytoplasmic surface of mitochondria (2,4,5). On the other hand, in yeast, most of the tRNA species were found to be

*To whom correspondence should be addressed. Tel: +81 3 5841 4392; Fax: +81 3 5841 8057; Email: nureki@biochem.s.u-tokyo.ac.jp

aminoacylated in the nucleus (6). These findings suggested that tRNA maturation also occurs in the cytoplasm, and the cytoplasmic tRNAs are imported into the nucleus by a retrograde pathway (7), which is either directly or indirectly mediated by the importin Mtr10p (8). Besides the aminoacylation-independent primary export pathway, a secondary re-export pathway exports tRNAs, which are then imported by the retrograde pathway in an aminoacylation-dependent manner (6,9).

The primary role of the retrograde import of tRNA was considered to be a quality control step for the aminoacylatable cytosolic tRNAs (10–13). In addition, this tRNA trafficking pathway between the nucleus and the cytoplasm plays an important role in nutrient-related regulation of cell growth to control translational efficiency. Indeed, recent studies showed that nitrogen source starvation in yeast causes the nuclear accumulation of imported mature tRNAs, to attenuate gene expression in the cytoplasm (7,8,14). Similar retrograde and re-export pathways of tRNA are also conserved in mammalian cells (15). Furthermore, these pathways are involved in various cellular functions in mammals, such as cell cycle regulation (16–18) and the nuclear translocation of the human immunodeficiency virus-1 replication complex (19).

Recent studies have provided insights into the molecular mechanism of the re-export pathway of aminoacylated tRNA. In yeast, the nuclear export receptor Msn5p is involved in the aminoacylation-dependent tRNA re-export process (20). Msn5p recognizes and re-exports aminoacylated tRNA, which is then delivered to eukaryotic elongation factor 1α (eEF-1α). Subsequently, eEF-1α carries the aminoacylated tRNA to the ribosome, to promote translation. The crystal structure of an Msn5p homologue, human exportin-5, in the complex with pre-microRNA was reported (21). Los1p, another nuclear export receptor for tRNA, participates in both the primary export and the aminoacylation-dependent re-export pathways, involving guanosine-5'-triphosphate (GTP) hydrolysis in RanGTPase/Gsp1p. Recently, the crystal structure of a Los1p homologue, Xpot, in complex with Gsp1p and tRNA was reported (22), providing structural insight into the tRNA export mechanism.

In this re-export pathway mediated by Los1p, cytoplasmic export protein (Cex1p) reportedly plays an important role in channeling the aminoacylated tRNA. A previous study demonstrated that disruptions of the Cex1p and eEF-1α or Los1p genes significantly reduced the efficiency of nuclear tRNA export, and that the double knockout of Cex1p and eEF-1α impaired cell growth (23). In addition, TAP and pull-down analyses revealed that Cex1p was co-purified with Los1p, Gsp1p, eEF-1α and the NPC component of Nup116p (23). Thus, these findings supported the channeling mechanism of tRNA, in which Cex1p captures mature aminoacylated tRNAs from Los1p on the cytoplasmic side of the NPC, and it delivers them to eEF-1α. Furthermore, a recent study revealed that Cex1p also regulates the GTPase activation of Gsp1p, by mediating the interaction between Gsp1p and a GTPase-activating protein, RanGAP/Rna1p in the different manner from Ran-binding protein family (24). This observation suggested that Cex1p is also important for Rna1p recruiting to the NPC, thereby enabling the dissociation of the Los1p•tRNA•Gsp1p export complex. These Cex1p functions are also conserved in higher eukaryotes, including human (25). Despite the important role of Cex1p for tRNA re-export pathway, the structural basis remains elusive.

To understand the molecular mechanism of tRNA transport system, we solved the crystal structure of C-terminal truncated Cex1p [Cex1pΔC-surface entropy reduction (SER)] from *Saccharomyces cerevisiae* at 2.2 Å resolution. Our structure revealed that Cex1p adopts an elongated architecture consisting of an amino-terminal kinase-like domain and a carboxyl-terminal HEAT domain containing 6 HEAT repeats. Combined with gel-shift and pull-down assays, the crystal structure enabled us to construct a model of the tRNA channeling complex comprising Los1p, Gsp1p, Cex1p and tRNA.

MATERIALS AND METHODS

Cloning, expression and purification of proteins

To solve the crystal structure, we truncated the C-terminal region of Cex1p (residues 565–761), which was predicted to be structurally disordered, and introduced point mutations predicted by the surface entropy reduction method (26) to facilitate the crystallization (Cex1pΔC-SER). The synthetic genes encoding yeast Cex1p mutants were cloned into a modified pET28b vector containing an N-terminal His tag and an HRV3C protease cleavage site for the tag removal. The native His–Cex1p mutants for biological assays were transformed into *Escherichia coli* strain BL21 (DE3) Star2 CodonPlus (Stratagene), and the cells were grown in Luria-Bertani (LB) medium. For the phase determination of the Cex1pΔC-SER structure, we used *E. coli* strain B834 (DE3) CodonPlus (Stratagene) grown in minimal medium (M9), in which the methionine was replaced with selenomethionine. The protein was overexpressed by culturing the cells for 15 h at 20°C with 0.5 mM isopropyl-β-D-thiogalactopyranoside (IPTG) induction. The cells were harvested and sonicated in lysis buffer, containing 20 mM Tris–HCl (pH 8.0), 500 mM NaCl, 5 mM $MgCl_2$, 1 mM β-mercaptoethanol (β-ME), 0.1 mM phenylmethylsulfonyl fluoride, 20 mM imidazole and 5% glycerol. The cell debris were removed by centrifugation at 13 500 r.p.m. for 30 min at 4°C. The supernatant was loaded onto a Ni-nitrilotriacetic acid (NTA) affinity column (QIAGEN) and eluted with 300 mM imidazole. The eluted fraction was dialyzed against 20 mM Tris–HCl buffer (pH 8.0) containing 2 mM $MgCl_2$, 1 mM β-ME, 50 mM NaCl and 5% glycerol. Only for Cex1pΔC-SER, to remove the His tag, the protein was incubated with the human rhinovirus Turbo-3C protease at 4°C overnight and re-loaded on a 2nd Ni-NTA column, and the flow-through was collected. The protein was loaded onto a Resource Q anion exchange column (GE Healthcare) and was eluted with a linear gradient of 50–1000 mM NaCl. The protein was finally purified by chromatography on a Superdex 20 030/100 size-exclusion column (GE Healthcare) eluted with gel filtration buffer, containing 20 mM Tris–HCl (pH 8.0), 2 mM $MgCl_2$,

1 mM dithiothreitol (DTT) and 100 mM NaCl. The fractions were concentrated to 6 mg/ml. The purity of the protein was monitored by sodium dodecyl sulfate–polyacrylamide gel electrophoresis (SDS–PAGE) and ultraviolet (UV) spectroscopy. About 2 mg of purified protein was obtained from 1 l cell culture. The protein sample was stored at −80°C until use. For the pull-down assay, we cloned yeast Los1p and Gsp1p into pGEX-6P1 vector (GE Healthcare). *E. coli* BL21 (DE3) Rosetta2 Codon Plus with pGEX-6P1-LOS1 and pGEX-6P1-GSP1 were grown at 37°C until the culture reached an A_{600} of 0.7 in LB medium. We applied the same protein preparation method for Both Los1p and Gsp1p. The protein expression was induced with 0.5 mM IPTG for 15 h at 20°C. The cells were resuspended and sonicated in lysis buffer, and the cell debris were removed by centrifugation at 13 500 r.p.m. for 30 min at 4°C. The supernatant was applied to a 2 ml Glutathione Sepharose Fast Flow column (GE Healthcare), which was washed with lysis buffer. Glutathione s-transferase (GST)–Los1p and GST–Gsp1p were eluted from the resin using GST elution buffer containing 20 mM reduced glutathione and 1 mM DTT. The fraction was diluted 10-fold by 20 mM Tris–HCl buffer (pH 8.0), containing 2 mM $MgCl_2$ and 1 mM DTT (ResQ buffer A), and the GST fusion proteins were loaded directly onto a Resource Q column, which was eluted with a linear gradient of 50–1000 mM NaCl. The fractions containing the pure proteins were concentrated and stored at −80°C until use. In addition, we prepared yeast MetRS for the aminoacylation of $tRNA^{Met}$. We co-expressed MetRS with its scaffolding protein, Arc1p to increase the solubility of the recombinant protein expressed in *E. coli*. The MetRS gene was synthesized by Genscript with codon optimization and was subcloned into pET20b (Novagen). The recombinant plasmids pET-20b–His–MetRS and pET-28b–His–Arc1p were co-transformed into *E. coli* BL21 (DE3) Rosetta2 Codon Plus. The strain was grown at 37°C until the culture reached an A_{600} of 0.7 in LB medium containing 30 μg/ml chloramphenicol, 50 μg/ml ampicillin and 50 μg/ml kanamycin. The protein was expressed and purified by Ni^{2+} affinity chromatography, as described for the Cex1p mutants. The eluted fraction was dialyzed against 20 mM Tris–HCl buffer (pH 8.0), containing 2 mM $MgCl_2$, 1 mM β-ME, 50 mM NaCl and 5% glycerol, and then loaded on a Resource Q anion exchange column (GE Healthcare). The protein was eluted with a linear gradient of 50–1000 mM NaCl. The fraction was diluted 10-fold with ResQ buffer A. To isolate MetRS from Arc1p, the eluate was loaded onto a Hitrap Heparin column (GE Healthcare), which was eluted with a linear gradient of 50–1000 mM NaCl. The purified protein was concentrated and stored at −80°C until use.

Crystallization

Initial screening for crystallization conditions was performed with several screening kits purchased from Hampton Research, as well as the MemSys and MemStart kits (Molecular Dimensions). The crystallization robots Hydra II Plus-One (Matrix Technologies) and Mosquito (TTP LabTech) were used for the initial crystallization screen, by the sitting-drop vapor-diffusion method at 293 K. In the initial crystallization screen, 0.1 μl of the protein solution was mixed with 0.1 μl of the mother liquor. For the crystallization of the selenomethionine-labeled Cex1p, the protein was concentrated to 4–6 mg/ml. Under the optimized crystallization conditions, 1 μl of the protein solution was mixed with 1 μl of crystallization solution and equilibrated against 500 μl of reservoir solution. We applied the in-gel crystallization technique (27) to slowly grow the crystals without the effects of convection, which reduced the mosaicity of the crystal from 1.5° to 0.7°. The crystals grew in 7% PEG3350 (PEG; polyethylene glycol), 100 mM Na-tartrate, 3% isopropanol and 50 mM 4-1-piperazineethanesulfonic acid (pH 7.5). The obtained crystals were briefly transferred to 1.2× reservoir solution containing 25% (w/v) glycerol and were flash-cooled by a cryo-stream of nitrogen gas at 100 K.

Data collection and processing

The data set of the crystal was collected at 100 K under a cold nitrogen stream with an oscillation range per image of 1°, using a Rayonix MX225HE detector on beamline BL41XU at SPring-8. The Se-Met Cex1p crystals diffracted up to 2.2 Å resolution. The resulting data set was processed with the program suite HKL2000 (HKL Research). The crystals belong to the primitive monoclinic space group $P2_1$, with unit-cell parameters $a = 34.1$, $b = 182.6$, $c = 112.3$ Å, $\beta = 98.9°$.

Structure determination

The phases of the Cex1p crystals were determined from multiple anomalous diffraction data sets collected from a single crystal of selenomethionine-derivatized Cex1pΔC-SER, which diffracted up to 2.2 Å resolution. The peak data set was used to determine the locations of the selenium atoms, using the program SHELXC/D (28). Several trials revealed 12 peaks among the 14 potential selenium sites expected in the asymmetric unit. Subsequent refinements of the heavy atom parameters and phase calculations were performed with the program SHARP (29). The data collection and phasing statistics are shown in Table 1. The initial phases were improved by density modification with RESOLVE (30). The initial model, containing 75% of all residues, was automatically built with RESOLVE. The model was further built manually using Coot (31). The diffraction data set analysis using the program Phenix.xtriage (32) indicated that the crystal was pseudomerohedrally twinned with a twining fraction of 0.43. The structure was refined using the twin target function implemented in the program REFMAC5 (33). The resulting twinning fraction was 0.425 for the twinning operator $(-h, -k, h+l)$. Refinement statistics are provided in Table 2.

Preparation of tRNAs

The tRNAs used for the gel-shift analysis with Cex1p were prepared as follows. $tRNA^{Phe}$ΔASL, in which most of the anticodon arm was deleted and replaced with an UUCG tetraloop, was transcribed (Supplementary Figure S3).

Table 1. Data collection and phasing statistics

	Cex1p ΔC-SER (SeMet)		
Data collection			
Space group	$P2_1$		
Cell dimensions			
a, *b*, *c* (Å)	34.1, 182.6, 112.3		
α, β, γ (°)	90, 98.9, 90		
	Peak	Inflection	High-remote
Wavelength (Å)	0.97914	0.97941	0.96410
Resolution (Å)[a]	50–2.2 (2.24–2.2)	50–2.33 (2.37–2.33)	50–2.29 (2.33–2.29)
R_{sym}[a]	0.099 (0.630)	0.099 (0.369)	0.102 (0.415)
<I>/<sigma(I)>[a]	36.1 (3.6)	28.5 (3.8)	24.0 (2.9)
Unique reflections[a]	67 587 (3029)	57 306 (2865)	60 128 (2927)
Completeness (%)[a]	98.9 (88.5)	99.9 (99.6)	99.7 (99.1)
Redundancy[a]	14.5 (9.9)	9.8 (6.3)	8.9 (5.0)

[a]The numbers in parentheses are for the last shell.

Table 2. Structure refinement statistics

	Cex1p ΔC-SER (SeMet)
Refinement	
Resolution (Å)	50–2.2
Number of reflections	60 925
R_{work}/R_{free}	0.1657/0.2067
Coordinate error based on free R-value	0.037
Number of atoms	
Protein	8364
Water	458
B-factors (Å^2)	
Protein	35.67
Water	39.24
R.m.s deviations	
Bond lengths (Å)	0.015
Bond angles (°)	1821
Ramachandran plot	
Most favored (%)	97.7
Allowed region (%)	2.1
Disallowed region (%)	0.2

The *S. cerevisiae* $tRNA^{Met}$ and $tRNA^{Phe}\Delta ASL$ genes were cloned into the pUC18 vector. The templates, linearized with BstNI, were transcribed *in vitro* with T7 RNA polymerase and purified under denaturing conditions by PAGE. The tRNAs were further purified by Resource Q anion-exchange chromatography (GE Healthcare). The purified tRNAs were dissolved in gel filtration buffer, and they were heated at 70°C for 10 min for refolding. The transcribed $tRNA^{Met}$ was methylated at 37°C for 30 min, in a reaction mixture containing 100 mM Tris–HCl, pH 8.0, 20 mM KCl, 10 mM $MgCl_2$, 2 mM DTT, 1 mM spermine, 2 mM adenosine triphosphate (ATP), 30 μM non-labeled L-methionine, 2 μM $tRNA^{Met}$ and 0.5 μM recombinant *S. cerevisiae* MetRS. An equal volume of phenol/chloroform/isoamyl alcohol (pH 5.2) was then added to the reaction mixture, which was vortexed vigorously and centrifuged at 15 000 r.p.m. for 15 min. The upper layer was precipitated with ethanol, rinsed with 70% ethanol, dissolved in 10 mM sodium acetate (pH 5.0) and then stored at −80°C. The aminoacylation efficiency of yeast MetRS was examined by standard methods using [^{35}S]-methionine solution, as described previously (34).

tRNA gel-shift analysis

Wild-type Cex1p or its mutants and tRNA molecules were incubated in 50 mM Tris–HCl (pH 8.8), containing 100 mM NaCl and 10 mM $MgCl_2$ for 1 h at 4°C, in a 20 μl reaction mixture. The tRNAs concentration was 20 μM, and the Cex1p mutant concentration was 10 μM. The reaction mixtures were supplemented with 1 μl of 6× loading buffer (Takara), loaded onto a 5% native polyacrylamide gel and fractionated for 150 min at 80 V. After electrophoresis, the gel was stained with SYBR Green II (Takara) and SimplyBlue SafeStain (GE Healthcare) to detect the nucleic acids and protein, respectively.

Pull-down assay

The Cex1p mutants (200 pmol) containing an N-terminal His tag and GST-fused Los1p and Gsp1p were incubated in binding buffer, containing 20 mM Tris–HCl (pH 8.0), 100 mM NaCl, 0.1% NP-40 (w/v) and 1 mM DTT, for 10 min at 25°C, in the presence or absence of an equal molar ratio of $tRNA^{Met}$ or GTP. The reaction mixture was added to 30 μl Glutathione Sepharose Fast Flow resin (GE Healthcare), and the volume was adjusted to 100 μl with binding buffer. The resin was incubated for 2 h at 4°C and washed five times with 300 μl binding buffer, and then 40 μl of SDS loading dye was added to the resin. The samples were boiled and resolved by SDS–PAGE. The gels were stained with SimplyBlue SafeStain (GE Healthcare) or subjected to anti-His western blotting and scanned with a Typhoon scanner (GE Healthcare).

Analytical ultracentrifugation

Sedimentation velocity experiments were performed with an Optima XL-I analytical ultracentrifuge (Beckman-Coulter). Samples (400 μl) in 20 mM Tris–HCl, pH 8.0, 150 mM NaCl, 5 mM $MgCl_2$ and 1 mM DTT were loaded into double sector centerpieces mounted in a Beckman An-50Ti rotor. The concentration profiles of the samples were monitored by the absorbance at 280 nm, without intervals between successive scans. The data were analyzed by the SEDFIT program (35) to obtain the c(s) profiles. On the basis of the assumption that the frictional ratio f/f_0 was common to all of the molecular species, c(s) was converted to obtain the molecular mass distribution function, c(M), using the implemented function in SEDFIT.

Sedimentation equilibrium experiments were carried out in an Optima XL-I analytical ultracentrifuge, using a 4-hole An60Ti rotor at 20°C with a standard double sector centerpieces and quartz windows. A quantity of 120 μl of each sample with the absorption of 0.2, 0.3 and 0.5 at 280 nm was applied in the sample hole, and the corresponding dialysate was loaded in the reference hole of the cell. The concentration gradients of the samples were monitored by absorption at 280 nm. The rotor speeds were 8800 r.p.m. for 24 h, 12 600 r.p.m. for 20 h

and 22 000 r.p.m. for 20 h. Scans were made every 2 h, and the equilibrium of the system was assumed when the last three scans were identical. Totally, nine data sets were globally fitted to a single species model to determine the weight-average molecular weight by the non-linear least-square fitting, as implemented in the Beckman Coulter software package.

Circular dichroism spectroscopy

CD spectra were measured on a J-720 spectropolarimeter (Jasco) at 20°C. Protein concentration of the sample was in the range of 0.1–0.2 mg/ml in 20 mM Tris–HCl, pH8.0, 150 mM NaCl, 5 mM $MgCl_2$ and 1 mM DTT. The same buffer was used as a reference solution. All the spectra were calculated as an average of four scans from 198 to 260 nm in a 1-mm path-length quartz cuvette (Hellma).

RESULTS AND DISCUSSION

Structure determination

We determined the crystal structure of yeast Cex1pΔC-SER, consisting of residues 9–564 and harboring the E535A, K536A and E537A mutations, at 2.2 Å resolution, by the multiple wavelength anomalous diffraction method, using selenomethionine derivatized crystals. The final model of CexΔC-SER except for the disorder region was refined to an *R*-factor of 16.6% (R_{free} = 20.7%). The tertiary structure of Cex1pΔC-SER consists of an amino-terminal kinase-like domain, a linker region and six C-terminal HEAT repeats (H1–H6) (Figure 1). The SER mutation is located on the C-terminal helix of a HEAT repeat, and it indeed improved the crystal packing interactions. Residues 545–564 and 311–319 were structurally disordered.

Cex1p has an inactive kinase-like domain

According to a structural similarity research using the Dali server (36), the N-terminal region (residues 9–235) of Cex1p most closely resembles the rearranged during transfection (RET) receptor tyrosine kinase (Figure 2a and b). The RET kinase is a single-pass transmembrane receptor, and its activation is essential for the development, cellular survival and regeneration of many neuronal populations (37). The structure of the RET kinase is composed of the N-terminal lobe, containing a five-stranded β-sheet, connected by the hinge loop to an α-helical C-terminal lobe (Figure 2b). The ATP binding pocket is formed in the interface between these two lobes (Figure 2b). Activation of the RET kinase on ligand binding facilitates receptor dimerization, which induces autophosphorylation of specific tyrosine residues in the A-loop (Figure 2b).

A comparison between the RET kinase and the kinase-like domain of Cex1p revealed that Cex1p shares a similar N-to-C lobe configuration to that of the RET kinase (Figure 2a and b). However, Cex1p has neither the ATP binding pocket nor the A-loop. In the structure of the RET kinase, the hinge loop, which connects the N- and C-lobes, interacts with the protruded loop in the C-lobe, forming a binding pocket for the adenine moiety of the ATP substrate (Figure 2d). In contrast, in the Cex1p structure, the hinge loop does not interact with the

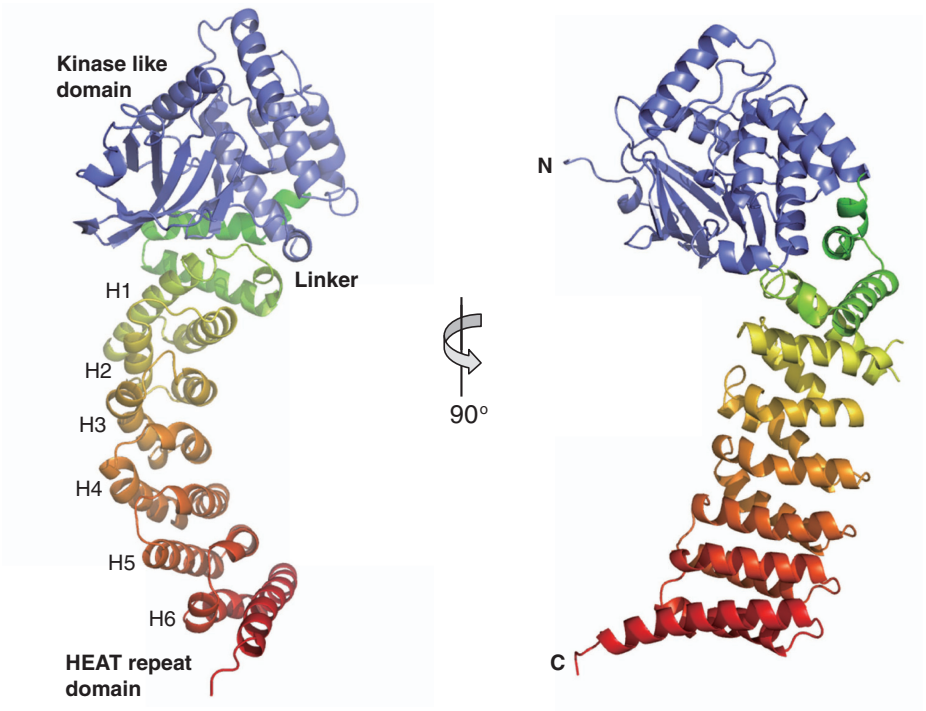

Figure 1. Overall structures of Cex1p.a. The monomeric structure of Cex1p is shown as a ribbon model, consisting of the kinase-like domain (9–235, blue), the linker region (236–290, green) and the HEAT repeat domain (291–544). The HEAT repeat domain is shown with a color gradient from yellow (N-terminus) to red (C-terminus). Figures were generated with CueMol (http://www.cuemol.org/) and PyMOL (Delano Scientific).

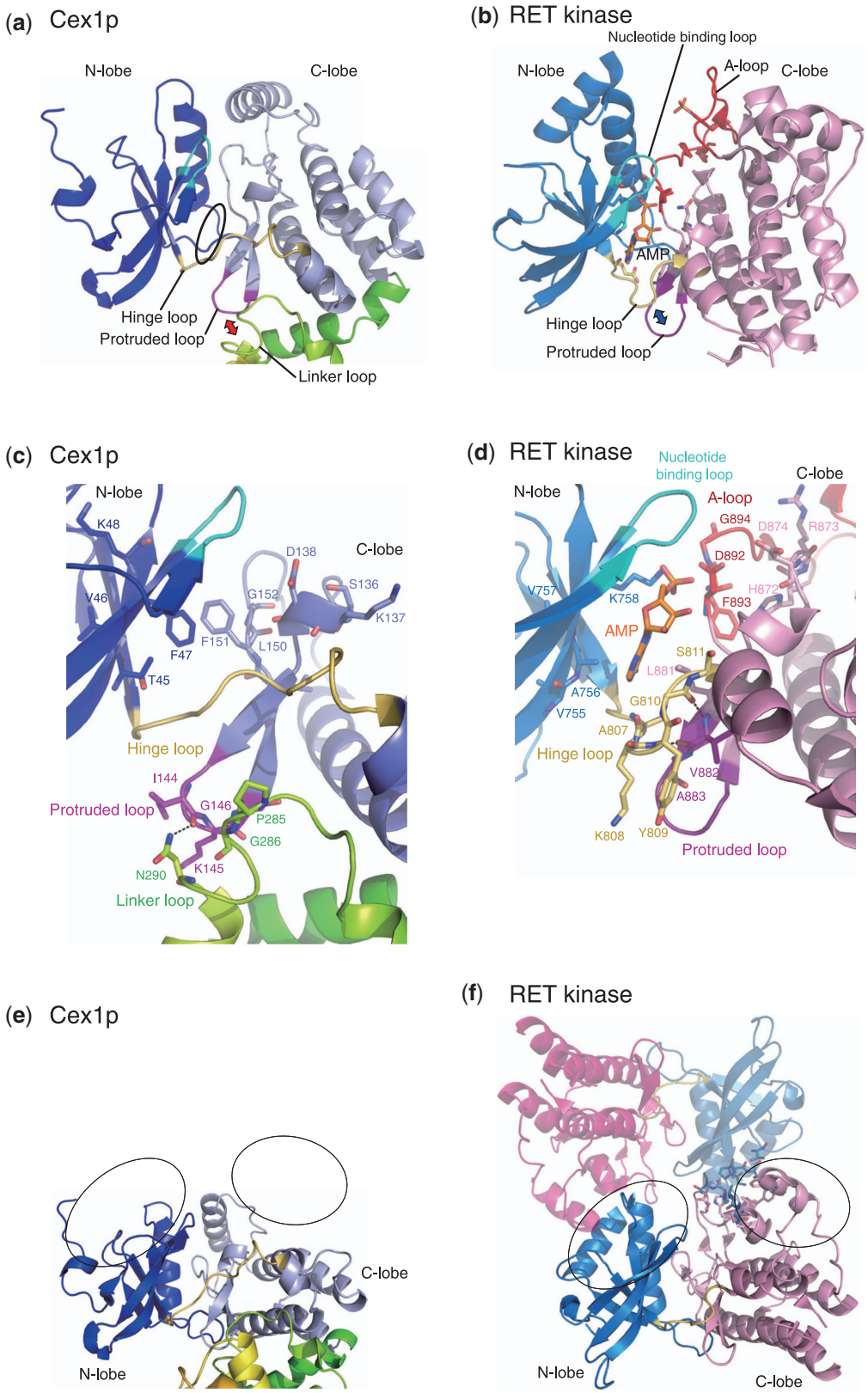

Figure 2. Comparison of RET kinase and the kinase-like domain of Cex1p. (**a**, **b**) The kinase-like domain of Cex1p (a) and RET kinase (b) are shown as ribbon models. The kinase-like domain of Cex1p consists of an N-lobe (9–92, blue) and a C-lobe (103–235, gray–blue). The N-lobe (713–805), C-lobe (812–1013) and A-loop (900–905) of RET kinase are colored light blue, light pink and red, respectively. Cex1p and RET kinase both contain a nucleotide binding loop (Cex1p: 26–30, RET: 731–736), hinge (Cex1p: 93–102, RET: 806–811) and protruded loop (Cex1p: 143–102, RET: 882–887), shown in cyan, yellow and purple, respectively. The protruded loop in RET kinase contacts the hinge loop (highlighted with the blue arrow). In contrast, the protruded loop in the kinase-like domain of Cex1p contacts with the linker loop (highlighted with the red

(continued)

protruded loop, which instead interacts with the linker loop in the HEAT domain (Figure 2c). Consequently, the hinge loop collapses the space for the ATP-binding cleft between the N- and C-lobes (Figure 2c), suggesting that the ATP binding pocket is not conserved in Cex1p. The structural comparison further revealed that Cex1p also lacks all three motifs, VA(I/V)K, HRD and DFG, which are essential for the kinase activity (Figure 2c and d). In the RET kinase, the Lys residue in the VA(I/V)K motif interacts with the α and β phosphate groups of the ATP, thereby anchoring its orientation (Figure 2d). The Asp residue in the HRD motif acts as a catalytic base, deprotonating the tyrosine hydroxyl to nucleophilically attack the γ-phosphate group of ATP (Figure 2d). The Asp residue in the DFG motif binds the Mg^{2+} ions that coordinate the β and γ-phosphate groups of ATP in the ATP-binding pocket (Figure 2d) in the Cex1p structure, the VA(I/V)K, HRD and DFG motifs are replaced by the ^{45}TVFK^{48}, ^{150}LFG^{152} and ^{136}SKD^{138} sequences, respectively (Figure 2c). In particular, the side chains of Phe47 in the ^{45}TVFK^{48} sequence and Phe151 in the ^{150}LFG^{152} sequence of Cex1p protrude into the cleft corresponding to the ATP binding pocket in the RET kinase (Figure 2c). Moreover, the RET kinase forms a dimer involving the A-loop, on the phosphorylation of the Tyr residue within it (Figure 2f). The dimerization interface involving the A-loop in the RET kinase is also not conserved in Cex1p (Figure 2e). Therefore, these observations further support the notion that the ATP binding pocket is not conserved in Cex1p, and that the kinase-like domain of Cex1p lacks kinase activity.

A previous study reported that inactive kinases account for >2% of all eukaryotic gene products (38). Many of these kinases were shown to function in either the regulation of another functional kinase activity or as a scaffold for multi-protein complexes. In the human brain, the Cex1p homologue Scyl1 reportedly acts as a scaffold protein for several neural proteins, such as coilin protein, ataxin 1 and survival motor neuron protein (39,40). In addition, the deletion mutant of the N-terminal kinase-like domain of Scyl1 causes dysfunction of neuromuscular junctions, resulting in muscular atrophy such as in murine neurodegenerative disease (41). Therefore, the kinase-like domain of Cex1p may also play a key role in protein–protein assembly.

Cex1p has a positively charged patch on the HEAT repeat domain

The HEAT repeat is a structural motif found in various proteins, such as chromatin-remodeling factors, cohesin, SWI2/SNF2 (SWItch/Sucrose NonFermentable), DNA-damage–response protein kinases and the importin β superfamily (21,42,43), and it is involved in a variety of cellular processes. The HEAT repeat is composed of pairs of anti-parallel α helices. In the HEAT repeat of the exportin family members, the α helix on the concave side is important for the protein–protein and protein–nucleotide interactions. The crystal structures of the exportin family members (21,22) revealed that the positive patch on the concave side of the HEAT domain is important for tRNA binding (Supplementary Figure S1). Interestingly, the present Cex1p structure revealed a large positively charged patch on the concave side of the HEAT repeat domain, which contains the Lys371, Lys406, Lys449, Lys479, Lys490 and Arg522 residues (Figure 3). Thus, Cex1p may interact with tRNA through this positively charged patch as observed in the other family members. The B-factors of Cex1p structure suggests that the convex side of the HEAT domain of Cex1p is relatively flexible (~50 Å^2) (Figure 3b). As the cargo-induced conformational changes of HEAT repeats are observed in the previously reported Xpot–Gsp1p–tRNA structure (22), tRNA binding of Cex1p might enable the HEAT repeat to adopt the tRNA complementary curved conformation.

Although several structures of inactive kinase were reported (44), to our knowledge, no 3D structure of any pseudokinase combining HEAT repeat has been reported.

The positively charged patch and the C-terminal disordered region of Cex1p are involved in tRNA binding

To investigate the tRNA binding mechanism of Cex1p, we performed a gel-shift analysis using several tRNAs and a series of Cex1p mutants based on the present crystal structure. A previous study reported that at least 19 major tRNA species of yeast, including cytoplasmic tRNA^{Met}, were present in the aminoacylated form in the nucleus (6). In addition, another report showed that Los1p associates with tRNA, without recognizing the anticodon (22). Therefore, we first analyzed the ability of wild-type, full-length Cex1p to bind cytoplasmic yeast tRNA^{Met}, tRNA^{Phe} and the previously reported anticodon stem–loop (ASL) truncated tRNA^{Phe} (tRNA^{Phe}ΔASL) (Supplementary Figure S2) (22). The tRNA^{Phe} used for this analysis was prepared from yeast cells (Sigma) and contains all of the base modifications, whereas the tRNA^{Met} and tRNA^{Phe}ΔASL were prepared by *in vitro* transcription and lack base modifications. For tRNA^{Met}, we also examined both of the aminoacylated and non-aminocylated tRNAs. We also measured far-UV CD spectra of all of the Cex1p constructs and confirmed that all of the Cex1p constructs studied in the gel-shift assay retain the native structures (Supplementary Figure S4).

The gel-shift results showed that aminoacylation has no effect on the tRNA affinity of Cex1p *in vitro* (Figure 4a).

Figure 2. Continued
arrow), and the free hinge loop fills into the ATP binding pocket (enclosed in a black circle). (**c**, **d**) Close-up views of the catalytic site of the Cex1p kinase-like domain (c) and RET kinase (d) reveal that Cex1p lacks all three essential kinase motifs. In the Cex1p structure, the main chain carbonyl of I144 in the protruded loop hydrogen bonds with N290 in the linker loop (indicated by the black dashed line). (**e**, **f**) Dimer interface of the active RET kinase (f) and the kinase-like domain of Cex1p (e), in the same orientation. The kinase-like domain of Cex1p forms a monomer, as it lacks the essential residues contributing to dimer formation in RET kinase (enclosed in the black circle).

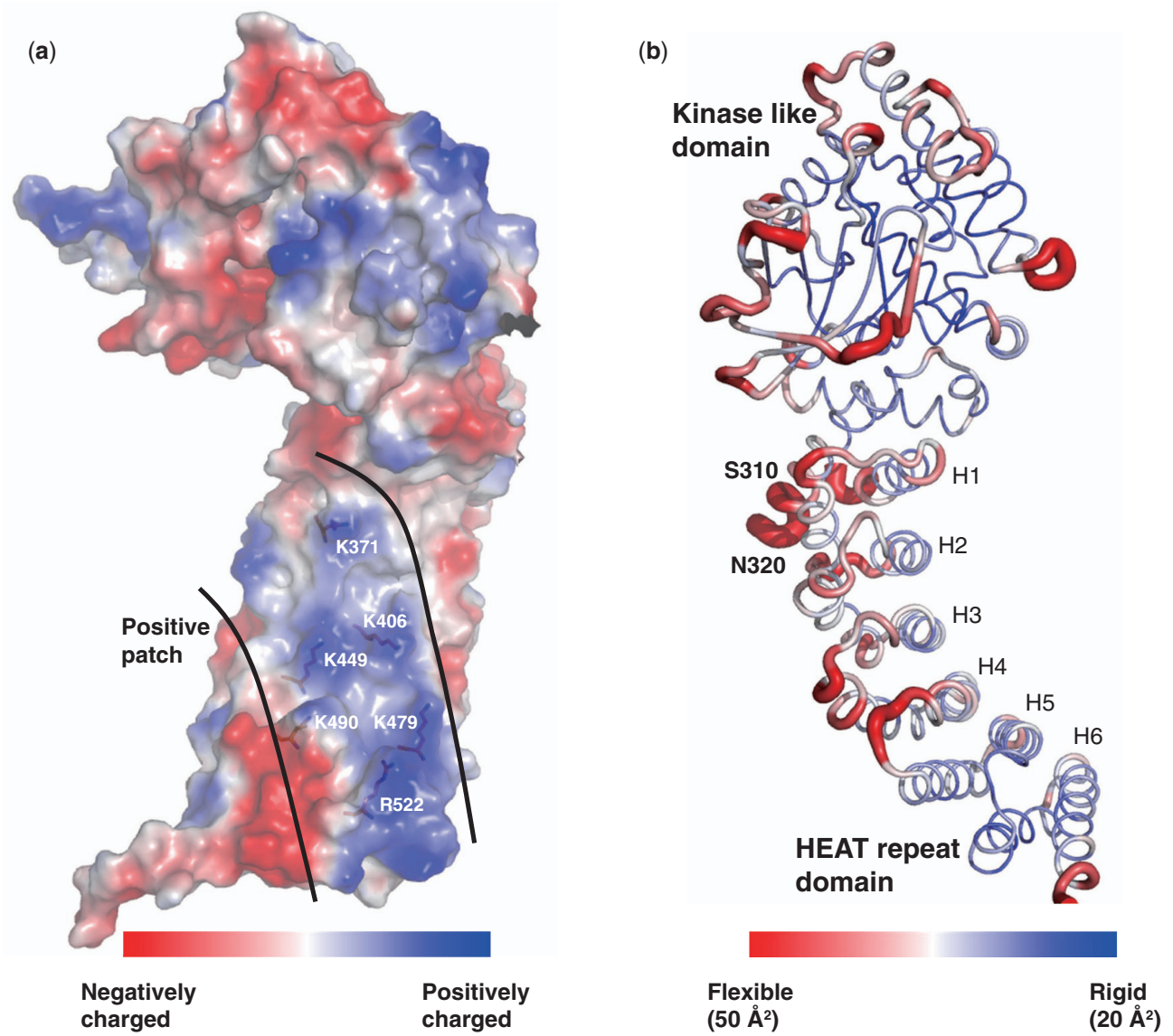

Figure 3. Architecture of the HEAT repeat domain of Cex1p. (**a**) Cex1p is shown as a solvent-accessible surface, colored according to the electrostatic potential (with positively charged residues in blue). Cex1p has a positively charged patch on the concave surface of the HEAT repeat domain, which consists of K371 in H2, K406 in H3, K449 in H4, K479 and K490 in H5 and R522 in H6 (shown as stick models). (**b**) Cex1p is shown as a ribbon model, colored by the B-factors. Blue represents low temperature factors (20 $Å^2$), whereas red represents high temperature factors (50 $Å^2$).

Similarly, the base modifications and the species of tRNA also did not affect the affinity for Cex1p (Figure 4a). In contrast, in the case of $tRNA^{Phe}$ΔASL, the amount of the bound tRNA was greatly reduced (Figure 4a), indicating the importance of the ASL for the tRNA recognition by Cex1p. Therefore, it is likely that Cex1p recognizes the sugar–phosphate backbone of tRNA, especially at the ASL.

Next, we performed a gel-shift analysis to identify the tRNA binding region of Cex1p, using the Cex1p mutants and non-aminoacylated cytoplasmic $tRNA^{Met}$. The CexΔC-SER mutant, which was used for the structure determination, bound $tRNA^{Met}$ in a similar manner to CexΔC, indicating that the SER mutation does not affect the tRNA binding by Cex1p (Figure 4b). The full-length Cex1p, which contains the disordered C-terminal region, exhibited a sharper band than CexΔC, indicating that the full-length Cex1p forms a more stable complex with tRNA than CexΔC (Figure 4a and b). In contrast, the N-terminal kinase-like domain of Cex1p (Cex1p9-358) exhibited no tRNA binding activity (Figure 4b). Thus, these results suggested that the HEAT domain of Cex1p is important for its tRNA binding ability, and that the C-terminal disordered region also has a significant impact on stable tRNA binding.

Next, we examined the effect of point mutations in the positively charged patch on the tRNA binding ability. The positively charged patch comprises the basic residues Lys371, Lys406, Lys449, Lys479, Lys490 and Arg522 (Figure 3a). Among them, Lys406 and Lys449 are well conserved among species (Supplementary Figure S3). The CexΔC protein bearing the K449A mutation

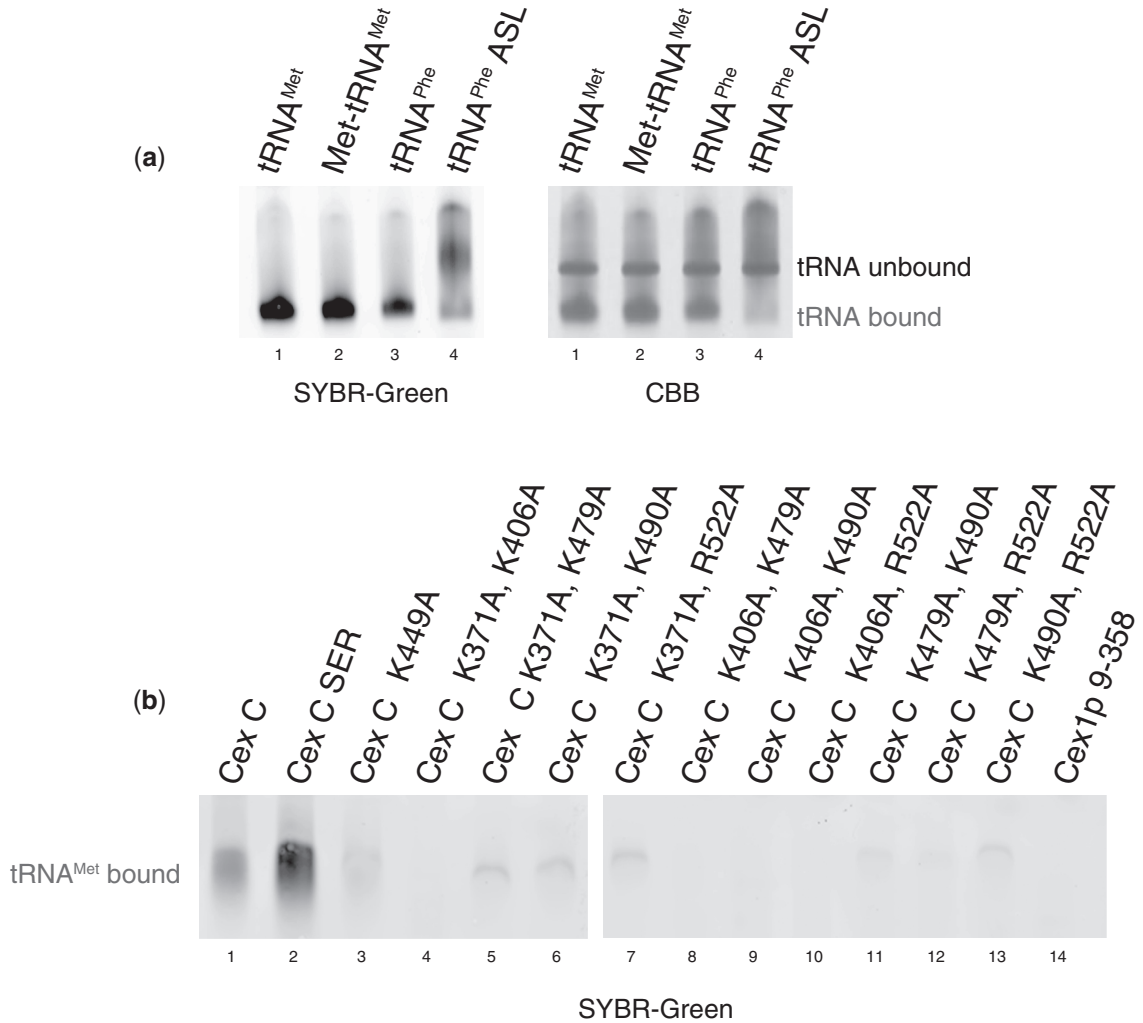

Figure 4. Electrophoretic mobility shift assay of tRNA binding by Cex1p. (**a**) Wild-type Cex1p (200 pmol) was incubated with a 2-fold molar excess of $tRNA^{Met}$ (lane 1), Met-$tRNA^{Met}$ (lane 2), $tRNA^{Phe}$ (lane 3) and $tRNA^{Phe}\Delta ASL$ (lane 4) at 4°C for 1 h, and the mixture was fractionated on a 5% polyacrylamide gel. The gel stained by SYBR Green II is shown on the left, and the gel stained by CBB is on the right. (**b**) The mixtures of $tRNA^{Met}$ and various Cex1p mutants were loaded onto the same type of non-denaturing polyacrylamide gel, which was stained by SYBR Green II.

abolished the tRNA binding activity (Figure 4b). Furthermore, double mutations in the positively charged patch (K371A/K406A, K371A/K479A, K371A/K490A, K371A/R522A, K406A/K479A, K406A/K490A, K406A/R522A, K479A/K490A, K479A/R522A and K490A/R522A) also drastically reduced the tRNA binding ability (Figure 4b). Thus, these results suggested that the positively charged patch on the HEAT repeat, especially including Lys449, is critically important for the tRNA binding ability.

The N-terminal part of Cex1p is important for its dimer formation and directly associates with the Los1p·Gsp1p export complex

To investigate the interaction between Cex1p and the tRNA export complex, we examined the binding ability of Cex1p mutants to the tRNA export complex, including Los1p, Gsp1p and/or tRNA, using GST pull-down analyses. The results showed that wild-type Cex1p binds Los1p, but not Gsp1p (Figure 5a). However, the presence of Gsp1p slightly enhanced the binding ability of Cex1p to Los1p (Figure 5a). In contrast, the presence of GTP and/or tRNA had no effect on the binding ability (Figure 5a). Therefore, these results suggested that, although Cex1p directly interacts with Los1p, the complex formation between Los1p and Gsp1p further enhances the interaction between Cex1p and Los1p. The truncation mutants, CexΔC, Cex1pΔC-SER and Cex1p9-358, still retained binding ability comparable with that of the wild-type Cex1p, whereas Cex1p591-761 did not bind to the Los1p*Gsp1p complex (Figure 5a). These results indicated that the N-terminal region encompassing residues Cex1p9-358 is critical for the binding of Cex1p to the tRNA export complex. Given that many inactive kinase-like domains function in protein–protein assembly networks (38), the Cex1p kinase-like domain is probably involved in the interaction between Cex1p and Los1p. Taken together, the present analyses suggested that

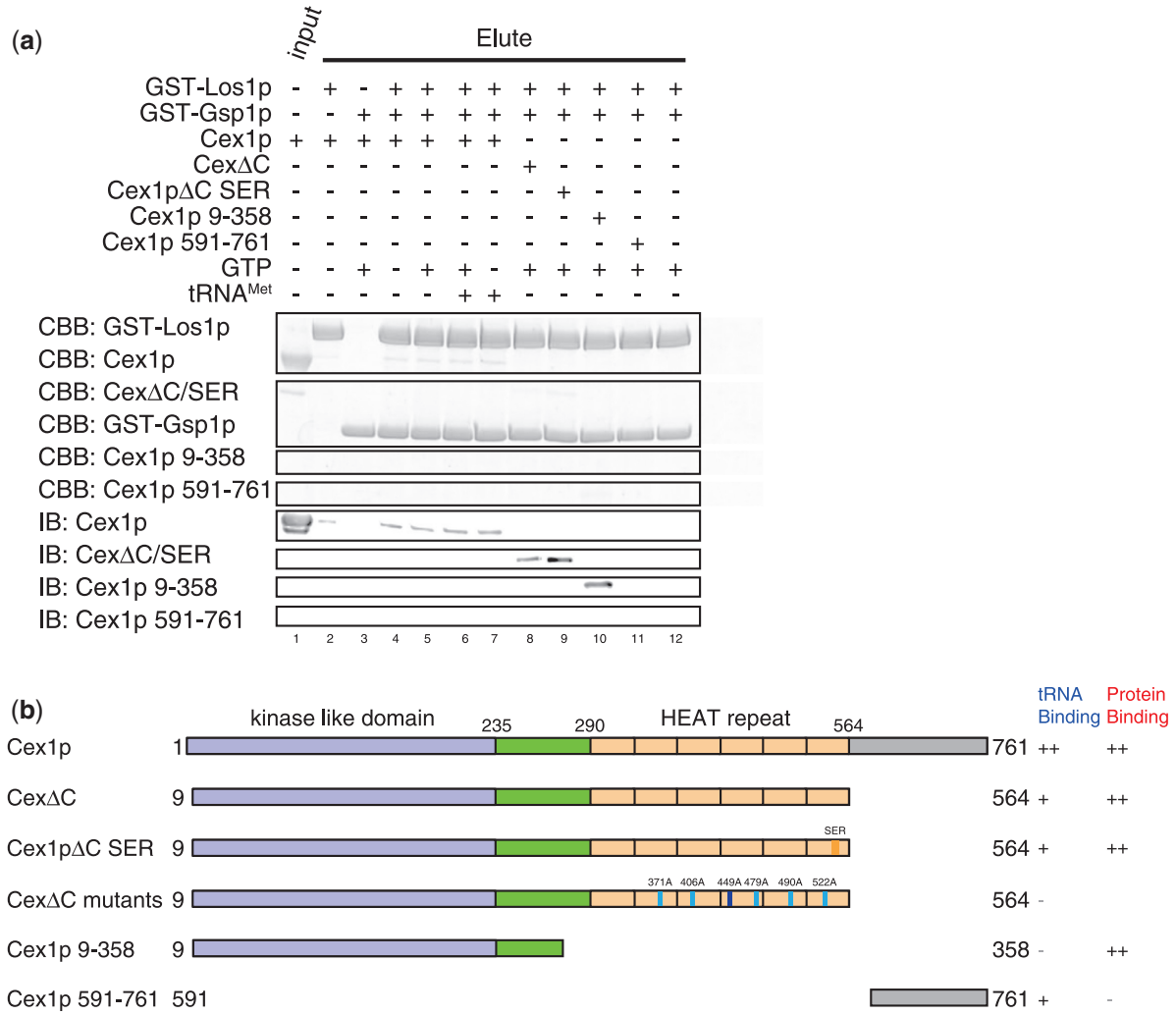

Figure 5. GST pull-down assay of GST-Los1p, GST-Gsp1p and His-Cex1p. (**a**) Cex1p mutants containing an N-terminal His tag were incubated with glutathione resin-bound GST-Los1p and GST-Gsp1p, and resolved by SDS–PAGE. CBB staining (the top row) and western blotting of the SDS–PAGE gel (the bottom row) were used to detect the bound Cex1p. Wild-type Cex1p interacted with Los1p (lane 2) and Los1p-Gsp1p, regardless of the presence or absence of $tRNA^{Met}$ and GTP (lanes 4–7). The Cex1p 9–564, 9–358 and CexΔC mutants also interact with Los1p-Gsp1p (lanes 8–11). (**b**) Schematic representation of the Cex1p mutants and summary of the gel-shift and pull-down analyses.

Cex1p interacts with Los1p in the tRNA export complex with its kinase-like domain, and then it captures the tRNA with its C-terminal region, including the HEAT domain, to shuttle the tRNA to eEF-1α(Figure 5b). Furthermore, we performed analytical ultracentrifugation experiments on Cex1p to investigate the dynamics of the Cex1p molecule in solution (Supplementary Figure S5). The results of the sedimentation velocity experiment showed that all of wild-type, Cex1pΔC-SER and Cex1p9-358 form a dimer in solution, and sedimentation equilibrium experiment confirmed that Cex1p9-358 forms a dimer. Although the asymmetric unit of our crystal contains two Cex1pΔC-SER monomers, the arrangement of the monomer is parallel in the crystal lattice and seems not physiological. These results suggest that kinase-like domain of Cex1p is also important for its dimer formation in solution, and the formation may contribute to associate with the Los1p•Gsp1p export complex. As the kinase-like domain of Cex1p lacks potential dimerization interface as observed in RET kinase, Cex1p possibly creates new dimer interaction surface to make complex formation with Los1p·Gsp1p export complex.

Possible model of the Los1p·Gsp1p·Cex1p·tRNA complex

To clarify the channeling mechanism of Cex1p, we compared the crystal structures of the Los1p•Gsp1p•tRNA complex from *Schizosaccharomyces pombe* and the EF-Tu•tRNA complex from *Thermus aquaticus*, the complex of a bacterial homologue of eEF-1α and an aminoacylated tRNA (aa-tRNA) (22,45). In the Los1p•Gsp1p•tRNA complex, the concave side formed by the HEAT repeats in Los1p recognizes the sugar–phosphate backbone of tRNA on its major groove and upper side (Figure 6a). On the other hand, in the crystal structure of EF-Tu•aa-tRNA, the 3′-CCA end of the aa-tRNA is bound to the specific pockets in the β-barrel structure of EF-Tu. EF-Tu uses this pocket to specifically recognize the aminoacyl moiety of the

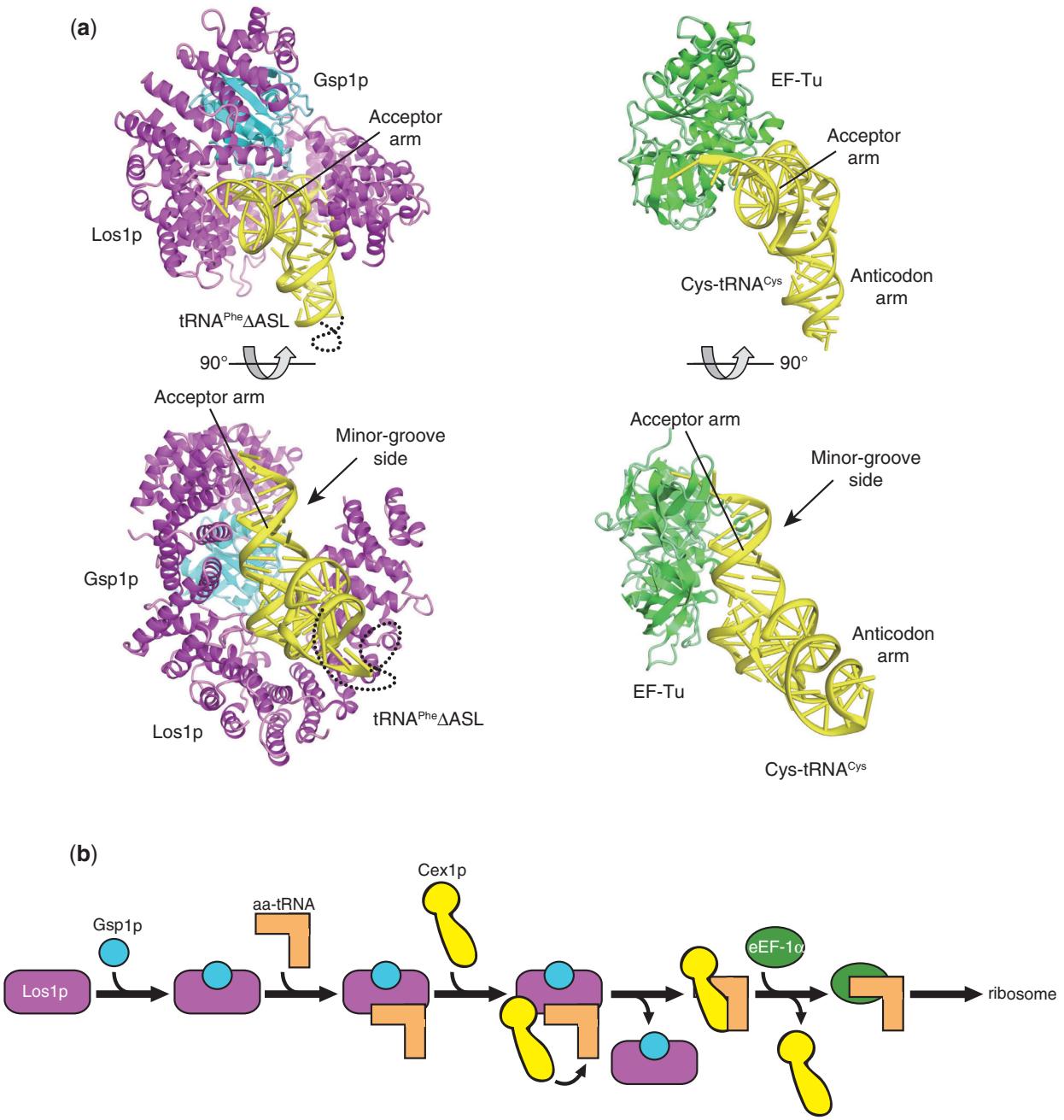

Figure 6. Possible model of the tRNA shuttling mechanism by Cex1p. (**a**) Ribbon models of the previously reported crystal structures of Los1p•Gsp1p•tRNA^{Phe}ΔASL (22) and EF-Tu•Cys-tRNA^{Cys} (45). Los1p, Gsp1p, EF-Tu and tRNAs are colored purple, cyan, green and yellow, respectively. The structurally disordered region of the anticodon tetraloop of tRNA^{Phe}ΔASL is shown by the red line. (**b**) Working model of the tRNA channeling mechanism by Cex1p.

aa-tRNA. Notably, EF-Tu also interacts with aa-tRNA on its major groove and upper side (Figure 6a). Our gel-shift and pull-down analyses revealed that Cex1p directly interacts with both of the tRNA (especially its ASL) and Los1p. Given that Cex1p forms complexes with both Los1p•Gsp1p•tRNA and eEF-1α•aa-tRNA, Cex1p probably accesses the tRNA on its minor groove and lower side, especially recognizing the ASL, and then shuttles the tRNA from Los1p to eEF-1α (Figure 6b).

CONCLUSION

The tRNA traffic between the nucleus and the cytoplasm is not unidirectional, and aminoacylation is used to select functional tRNAs for cytoplasmic export. We determined the crystal structure of CexΔC-SER, which revealed that Cex1p has an N-terminal kinase-like domain and a C-terminal elongated HEAT domain. The GST pull-down and analytical ultracentrifugation analyses showed that the kinase-like domain of Cex1p plays key roles in

binding to Los1p and in dimer formation. Furthermore, the gel-shift analysis showed that the positively charged patch on the HEAT domain and the C-terminal disordered region play essential roles in the tRNA binding. Considering these observations, we constructed a model for the tRNA channeling mechanism, in which the kinase-like domain of Cex1p interacts with Los1p in the tRNA export complex, whereas its HEAT domain and C-terminal disordered region interact with the tRNA, thereby capturing the aminoacylated tRNA from Los1p and delivering it to eEF-1α.

It was shown that Cex1p bind Gsp1p, which does not affect the GTPase activity of Gsp1p (24). Moreover, it is shown that the formation of the Los1p•tRNA•Gsp1p•GTP export complex is dependent on the presence of tRNA, and that this complex is resistant to Rna1p activation of the GTPase activity of Gsp1p (46). Thus, the export complex dissociation readily relies on the binding of Cex1p, as tRNA accumulation inside the nucleus (at restrictive temperature) can be observed in a cex1::kanMX, rna1-1 strain (a deletion of CEX1 and a its allele of RNA1), whereas it is much more difficult to observe in an rna1-1 strain. All together, this demonstrates the implication of Cex1p in export complex dissociation. In Figure 5a, the N-terminal kinase-like domain did not bind Gsp1p in the absence of Los1p, and one can extrapolate that binding of the N-terminal domain of Cex1p to the Los1p•Gsp1p•GTP complex is unable to promote its dissociation (lane 10), probably because of the absence of Rna1p and most probably tRNA to obtain a functional system. This means that Cex1p, especially the N-terminal kinase-like domain, may recruit Rna1p to the export complex and promote its dissociation, as described previously (24).

However, the means by which the aminoacylation state of tRNA is discriminated in the re-export pathway remains elusive. The crystal structure of the Los1p•Gsp1p•tRNA complex suggested that Los1p forms specific interactions with the 3′ single-stranded overhang of tRNA, whereas the 3′-terminal base, A76, twists away from Los1p and the adenosine moiety is exposed to the solvent. These observations precluded the possibility that Los1p discriminates between aminoacylated and non-aminoacylated tRNAs. On the other hand, our gel-shift assay results indicated that aminoacylation has little impact on the tRNA affinity of Cex1p *in vitro*. However, it is possible that Cex1p discriminates the aminoacyl moiety of the tRNA *in vivo*, but the difference in its affinities between the aminoacylated and non-aminoacylated tRNAs is too small to be detected by an *in vitro* gel-shift analysis. Alternatively, other protein component(s) may be involved in the discrimination of the aminoacylation state of tRNAs in the re-export pathway. Further studies, including the structural analysis of the Cex1p•tRNA complex, may be required for a complete understanding of the mechanism of the aminoacylation-dependent re-export pathway.

A recent study revealed that homologues of Cex1p from higher eukaryotes have functions other than tRNA trafficking. The mammalian homologue of Cex1p, telomerase transcriptional element-interacting factor (TEIF), reportedly binds to the hTERT promoter and stimulates its transcription and telomerase activities (47). TEIF can also enhance the transcriptional level of the β subunit of RNA polymerase, which is over-expressed in many human cancers (48). In particular, the kinase-like domain and the HEAT domain are also conserved in TEIF (Supplementary Figure S2). We speculate that the HEAT domain of TEIF is involved in DNA binding, in a similar manner to the HEAT domain of Cex1p. From such a viewpoint, further analyses based on the Cex1p structure will lead to new aspects of the pleiotropic functions of Cex1p homologues in higher eukaryotes.

ACCESSION NUMBERS

The PDB accession number of the new structure is 3VWA.

SUPPLEMENTARY DATA

Supplementary Data are available at NAR Online: Supplementary Figures 1–5.

ACKNOWLEDGEMENTS

The authors thank the beam-line staffs at BL41XU of SPring-8 (Harima, Japan) and NW12 of PF-AR (Tsukuba, Japan) for technical help during data collection.

FUNDING

Japan Society for the Promotion of Science (JSPS) through its 'Funding Program for World-Leading Innovative R&D on Science and Technology (FIRST) program' (to O.N., K.N. and Y.A.); Core Research for Evolutional Science and Technology (CREST) program 'The Creation of Basic Medical Technologies to Clarify and Control the Mechanisms Underlying Chronic Inflammation' of the Japan Science and Technology Agency (JST) (to O.N.); Grant-in-Aid for Scientific Research from the Ministry of Education, Culture, Sports, Science and Technology (MEXT) of Japan (to R.I. and O.N.); Université de Strasbourg, the Centre National de la Recherche Scientifique, the Agence Nationale de la Recherche [ANR-09-BLAN-0091-02]; National Program 'Ivestissement d'Avenir' (LabEx MitoCross). Funding for open access charge: Core Research for Evolutional Science and Technology (CREST) program 'The Creation of Basic Medical Technologies to Clarify and Control the Mechanisms Underlying Chronic Inflammation' of the Japan Science and Technology Agency (JST).

Conflict of interest statement. None declared.

REFERENCES

1. Bertrand,E., Houser-Scott,F., Kendall,A., Singer,R.H. and Engelke,D.R. (1998) Nucleolar localization of early tRNA processing. *Genes Dev.*, **12**, 2463–2468.

2. Huh,W.K., Falvo,J.V., Gerke,L.C., Carroll,A.S., Howson,R.W., Weissman,J.S. and O'Shea,E.K. (2003) Global analysis of protein localization in budding yeast. *Nature*, **425**, 686–691.
3. Van Hoof,A., Lennertz,P. and Parker,R. (2000) Yeast exosome mutants accumulate 3′-extended polyadenylated forms of U4 small nuclear RNA and small nucleolar RNAs. *Mol. Cell. Biol.*, **20**, 441–452.
4. Yoshihisa,T., Ohshima,C., Yunoki-Esaki,K. and Endo,T. (2007) Cytoplasmic splicing of tRNA in *Saccharomyces cerevisiae*. *Genes Cell.*, **12**, 285–297.
5. Takano,A., Endo,T. and Yoshihisa,T. (2005) tRNA actively shuttles between the nucleus and cytosol in yeast. *Science*, **309**, 140–142.
6. Steiner-Mosonyi,M. and Mangroo,D. (2004) The nuclear tRNA aminoacylation-dependent pathway may be the principal route used to export tRNA from the nucleus in *Saccharomyces cerevisiae*. *Biochem. J.*, **378**, 809–816.
7. Shaheen,H.H. and Hopper,A.K. (2005) Retrograde movement of tRNAs from the cytoplasm to the nucleus in *Saccharomyces cerevisiae*. *Proc. Natl. Acad. Sci. USA*, **102**, 11290–11295.
8. Hurto,R.L., Tong,A.H.Y., Boone,C. and Hopper,A.K. (2007) Inorganic phosphate deprivation causes tRNA nuclear accumulation via retrograde transport in *Saccharomyces cerevisiae*. *Genetics*, **176**, 841–852.
9. Phizicky,E.M. and Hopper,A.K. (2010) tRNA biology charges to the front. *Genes Dev.*, **24**, 1832–1860.
10. Lund,E. and Dahlberg,J.E. (1998) Proofreading and aminoacylation of tRNAs before export from the nucleus. *Science*, **282**, 2082–2085.
11. Sarkar,S., Azad,A.K. and Hopper,A.K. (1999) Nuclear tRNA aminoacylation and its role in nuclear export of endogenous tRNAs in *Saccharomyces cerevisiae*. *Proc. Natl. Acad. Sci. USA*, **96**, 14366–14371.
12. Grosshans,H., Hurt,E. and Simos,G. (2000) An aminoacylation-dependent nuclear tRNA export pathway in yeast. *Genes Dev.*, **14**, 830–840.
13. Azad,A.K., Stanford,D.R., Sarkar,S. and Hopper,A.K. (2001) Role of nuclear pools of aminoacyl-tRNA synthetases in tRNA nuclear export. *Mol. Biol. Cell*, **12**, 1381–1392.
14. Whitney,M.L., Hurto,R.L., Shaheen,H.H. and Hopper,A.K. (2007) Rapid and reversible nuclear accumulation of cytoplasmic tRNA in response to nutrient availability. *Mol. Biol. Cell*, **18**, 2678–2686.
15. Shaheen,H.H., Horetsky,R.L., Kimball,S.R., Murthi,A., Jefferson,L.S. and Hopper,A.K. (2007) Retrograde nuclear accumulation of cytoplasmic tRNA in rat hepatoma cells in response to amino acid deprivation. *Proc. Natl. Acad. Sci. USA*, **104**, 8845–8850.
16. Steiner-Mosonyi,M., Leslie,D.M., Dehghani,H., Aitchison,J.D. and Mangroo,D. (2003) Utp8p is an essential intranuclear component of the nuclear tRNA export machinery of *Saccharomyces cerevisiae*. *J. Biol. Chem.*, **278**, 32236–32245.
17. Strub,B.R., Eswara,M.B.K., Pierce,J.B. and Mangroo,D. (2007) Utp8p is a nucleolar tRNA-binding protein that forms a complex with components of the nuclear tRNA export machinery in *Saccharomyces cerevisiae*. *Mol. Biol. Cell*, **18**, 3845–3859.
18. Ghavidel,A., Kislinger,T., Pogoutse,O., Sopko,R., Jurisica,I. and Emili,A. (2007) Impaired tRNA nuclear export links DNA damage and cell-cycle checkpoint. *Cell*, **131**, 915–926.
19. Zaitseva,L., Myers,R. and Fassati,A. (2006) tRNAs promote nuclear import of HIV-1 intracellular reverse transcription complexes. *PLoS Biol.*, **4**, 1689–1706.
20. Murthi,A., Shaheen,H.H., Huang,H.-Y., Preston,M.A., Lai,T.-P., Phizicky,E.M. and Hopper,A.K. (2010) Regulation of tRNA bidirectional nuclear-cytoplasmic trafficking in *Saccharomyces cerevisiae*. *Mol. Biol. Cell*, **21**, 639–649.
21. Okada,C., Yamashita,E., Lee,S.J., Shibata,S., Katahira,J., Nakagawa,A., Yoneda,Y. and Tsukihara,T. (2009) A high-resolution structure of the pre-microrna nuclear export machinery. *Science*, **326**, 1275–1279.
22. Cook,A.G., Fukuhara,N., Jinek,M. and Conti,E. (2009) Structures of the tRNA export factor in the nuclear and cytosolic states. *Nature*, **461**, 60–65.
23. McGuire,A.T. and Mangroo,D. (2007) Cex1p is a novel cytoplasmic component of the *Saccharomyces cerevisiae* nuclear tRNA export machinery. *EMBO J.*, **26**, 288–300.
24. McGuire,A.T. and Mangroo,D. (2011) Cex1p facilitates rna1p-mediated dissociation of the Los1p-tRNA-Gsp1p-GTP export complex. *Traffic*, **13**, 234–256.
25. Chafe,S.C. and Mangroo,D. (2010) Scyl1 facilitates nuclear tRNA export in mammalian cells by acting at the nuclear pore complex. *Mol. Biol. Cell*, **21**, 2483–2499.
26. Goldschmidt,L., Cooper,D.R., Derewenda,Z.S. and Eisenberg,D. (2007) Toward rational protein crystallization: a web server for the design of crystallizable protein variants. *Protein Sci.*, **16**, 1569–1576.
27. Sauter,C., Dhouib,K. and Lorber,B. (2007) From macrofluidics to microfluidics for the crystallization of biological macromolecules. *Cryst. Growth Des.*, **7**, 2247–2250.
28. Schneider,T.R. and Sheldrick,G.M. (2002) Substructure solution with SHELXD. *Acta Crystallogr. D Biol. Crystallogr.*, **D58**, 1772–1779.
29. de La Fortelle,E. and Bricogne,G. (1997) Maximumlikelihood heavy-atom parameter refinement for multiple isomorphous replacement and multiwavelength anomalous diffraction methods. *Methods Enzymol.*, **276**, 472–494.
30. Terwilliger,T.C. (2003) SOLVE and RESOLVE: automated structure solution and density modification. *Macromol. Crystallogr.*, **374**, 22–37.
31. Emsley,P., Lohkamp,B., Scott,W.G. and Cowtan,K. (2010) Features and development of Coot. *Acta Crystallogr. D Biol. Crystallogr.*, **66**, 486–501.
32. Adams,P.D., Grosse-Kunstleve,R.W., Hung,L.-W., Ioerger,T.R., McCoy,A.J., Moriarty,N.W., Read,R.J., Sacchettini,J.C., Sauter,N.K. and Terwilliger,T.C. (2002) PHENIX: Building new software for automated crystallographic structure determination. *Acta Crystallogr. D Biol. Crystallogr.*, **58**, 1948–1954.
33. Murshudov,G.N., Vagin,A.A. and Dodson,E.J. (1997) Refinement of macromolecular structures by the maximum-likelihood method. *Acta Crystallogr. D Biol. Crystallogr.*, **53**, 240–255.
34. Karanasios,E., Boleti,H. and Simos,G. (2008) Incorporation of the Arc1p tRNA-binding domain to the catalytic core of MetRS can functionally replace the yeast Arc1p-MetRS complex. *J. Mol. Biol.*, **381**, 763–771.
35. Schuck,P. (2000) Size-distribution analysis of macromolecules by sedimentation velocity ultracentrifugation and lamm equation modeling. *Biophys. J.*, **78**, 1606–1619.
36. Holm,L. and Rosenstrom,P. (2010) Dali server: conservation mapping in 3D. *Nucleic Acids Res.*, **38**, W545–W549.
37. Schuchardt,A., Dagati,V., Larssonblomberg,L., Costantini,F. and Pachnis,V. (1994) Defects in the kidney and enteric nervous system of mice lacking the tyrosine kinase receptor Ret. *Nature*, **367**, 380–383.
38. Boudeau,J., Miranda-Saavedra,D., Barton,G.J. and Alessi,D.R. (2006) Emerging roles of pseudokinases. *Trends Cell Biol.*, **16**, 443–452.
39. Humbert,S. and Saudou,F. (2006) The ataxia-ome: connecting disease proteins of the cerebellum. *Cell*, **125**, 645–647.
40. Lim,J., Hao,T., Shaw,C., Patel,A.J., Szabo,G., Rual,J.F., Fisk,C.J., Li,N., Smolyar,A., Hill,D.E. *et al.* (2006) A protein-protein interaction network for human inherited ataxias and disorders of Purkinje cell degeneration. *Cell*, **125**, 801–814.
41. Schmidt,W.M., Kraus,C., Hoger,H., Hochmeister,S., Oberndorfer,F., Branka,M., Bingemann,S., Lassmann,H., Mueller,M., Macedo-Souza,L.I. *et al.* (2007) Mutation in the Scyl1 gene encoding amino-terminal kinase-like protein causes a recessive form of spinocerebellar neurodegeneration. *EMBO Rep.*, **8**, 691–697.
42. Neuwald,A.F. and Hirano,T. (2000) HEAT repeats associated with condensins, cohesins, and other complexes involved in chromosome-related functions. *Genome Res.*, **10**, 1445–1452.
43. Sibanda,B.L., Chirgadze,D.Y. and Blundell,T.L. (2010) Crystal structure of DNA-PKcs reveals a large open-ring cradle comprised of HEAT repeats. *Nature*, **463**, 118–121.
44. Zhang,H., Photiou,A., Grothey,A., Stebbing,J. and Giamas,G. (2012) The role of pseudokinases in cancer. *Cell. Signal.*, **24**, 1173–1184.

45. Nissen,P., Thirup,S., Kjeldgaard,M. and Nyborg,J. (1999) The crystal structure of Cys-tRNA(Cys)-EF-Tu-GDPNP reveals general and specific features in the ternary complex and in tRNA. *Structure*, **7**, 143–156.
46. Hellmuth,K., Lau,D.M., Bischoff,F.R., Künzler,M., Hurt,E. and Simos,G. (1998) Yeast Los1p has properties of an exportin-like nucleocytoplasmic transport factor for tRNA. *Mol. Cell Biol.*, **18**, 6374–6386.
47. Tang,Z.W., Zhao,Y.J., Mei,F., Yang,S.M., Li,X., Lv,J.J., Hou,L. and Zhang,B. (2004) Molecular cloning and characterization of a human gene involved in transcriptional regulation of hTERT. *Biochem. Biophys. Res. Commun.*, **324**, 1324–1332.
48. Zhao,Y.J., Zheng,H., Ling,Y., Hou,L. and Zhang,B. (2005) Transcriptional upregulation of DNA polymerase beta by TEIF. *Biochem. Biophys. Res. Commun.*, **333**, 908–916.